



## OPEN

# Combining stress transfer and source directivity: the case of the 2012 Emilia seismic sequence

## SUBJECT AREAS:

SEISMOLOGY

GEOLOGY

TECTONICS

STRUCTURAL GEOLOGY

Vincenzo Convertito<sup>1</sup>, Flaminia Catalli<sup>2</sup> & Antonio Emolo<sup>3</sup>

<sup>1</sup>Istituto Nazionale di Geofisica e Vulcanologia – Osservatorio Vesuviano, Via Diocleziano 328, 80124, Napoli, Italy, <sup>2</sup>Institute of Geophysics ETH Zurich, Schweizer. Erdbebendienst, Sonneggstrasse 5, 8092 Zurich, Switzerland, <sup>3</sup>Dipartimento di Fisica, Università degli Studi Federico II, Complesso Universitario di Monte S. Angelo, Edificio 6, via Cintia, 80126, Napoli, Italy.

Received  
20 March 2013

Accepted  
15 October 2013

Published  
1 November 2013

Correspondence and requests for materials should be addressed to V.C. (vincenzo.convertito@ov.ingv.it)

The Emilia seismic sequence (Northern Italy) started on May 2012 and caused 17 casualties, severe damage to dwellings and forced the closure of several factories. The total number of events recorded in one month was about 2100, with local magnitude ranging between 1.0 and 5.9. We investigate potential mechanisms (static and dynamic triggering) that may describe the evolution of the sequence. We consider rupture directivity in the dynamic strain field and observe that, for each main earthquake, its aftershocks and the subsequent large event occurred in an area characterized by higher dynamic strains and corresponding to the dominant rupture direction. We find that static stress redistribution alone is not capable of explaining the locations of subsequent events. We conclude that dynamic triggering played a significant role in driving the sequence. This triggering was also associated with a variation in permeability and a pore pressure increase in an area characterized by a massive presence of fluids.

The Emilia region, Northern Apennines, Italy, was struck by a seismic sequence that started on May 19, 2012, at 23:13:27 GMT with a  $M_w$  3.8 earthquake. It produced about 2100 events during the following month, affecting an area of about  $60 \text{ km} \times 30 \text{ km}$  elongated in the EW direction (Figure 1). The sequence began with the reactivation of two buried, sub-parallel  $N100^\circ E$ -striking thrust faults with hypocenters located mainly in the upper  $10 \text{ km}^1$ . The largest events,  $M_w$  5.6 and 5.4, occurred on May, 20 and 29, respectively, and were followed by 6  $M_w > 4.5$  earthquakes over the next 2 weeks.

This is a strategic area for the Italian economy and a site of intensive petroleum extraction<sup>2</sup> and gas storage (<http://unmig.sviluppoeconomico.gov.it/unmig/pozzi/completo.asp>). For this reasons, understand the physical processes involved in triggering of this seismic sequence, with particular attention on the role of fluids, and try to improve the risk assessment is particularly important in this part of Italy. In this study we investigate the static effect of the Coulomb stress redistribution and some dynamic effects of passing seismic waves.

## Results

We use 22 hypocentral locations, moment magnitudes and focal mechanism solutions<sup>3</sup> to estimate source dimensions<sup>4,5</sup> and cumulative changes in the static stress field ( $\Delta CFS$ ). In addition, we use peak-ground velocities (PGVs) of the 8 largest earthquakes (Table 1) to estimate: i) rupture directivity, and ii) the peak-dynamic strain field. Combining i) and ii) results in an original representation of the dynamic strain field, whose amplitude and azimuthal distribution is modified by source directivity. The PGVs used in this study are those also used to produce ShakeMaps in Italy<sup>6</sup>. The waveforms are recorded by the Italian permanent seismic network (<http://inside.rm.ingv.it>) and Rete Accelerometrica Nazionale (<http://www.protezionecivile.gov.it/jcms/it/ran.wp>). The combination of the two datasets provides data with a reliable azimuthal coverage of stations. According to the automatic procedures implemented at INGV<sup>6</sup>, seismograms are corrected by the instrumental response, and processed applying a de-trending and a band-pass filtering in the range 0.01–30 Hz. At each station, the PGV corresponds to the largest value between the two horizontal components of the recorded velocity. The number of PGV data available for each earthquake is reported in Figure 2 where only those seismic stations located at epicentral distances less than 150 km are included. Moreover, we discarded peak velocity values differing more than  $2\sigma$  from the predictions provided by the Ground-Motion Prediction Equation (GMPE)<sup>7</sup>, where  $\sigma$  is the standard error of the GMPE. This resulted in discarding about 18% on average, of available data.

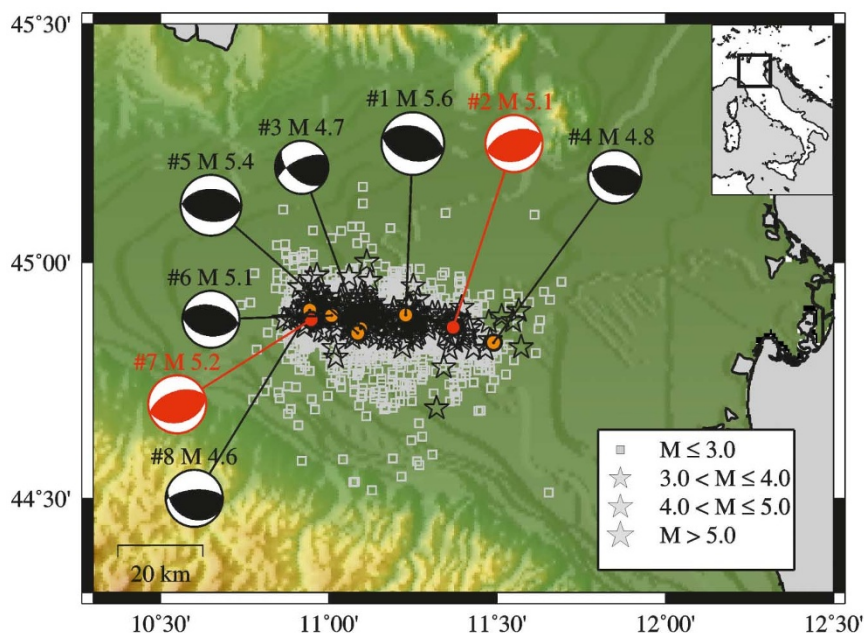


**Figure 1 | Location map of the 2012 Emilia earthquake sequence.** Geographic location of the 2012 Emilia seismic sequence (Italian Seismological Instrumental and parametric Data-basE, <http://iside.rm.ingv.it>). Orange dots, with corresponding focal mechanisms<sup>3</sup>, represent the epicenters of the main events analysed in this study and listed in Table 1. Red dots represent the location of events 2 and 7, whose focal mechanisms have been estimated by average of the known focal mechanisms. For each event the sequential number and magnitude are also specified. Open stars indicate location of events with  $M > 3.0$ , while gray squares represent all the other earthquakes. The sequence spans a time interval of about one month and covers an area of about  $60 \text{ km} \times 30 \text{ km}$ . The figure was generated by using the Generic Mapping Tools (<http://gmt.soest.hawaii.edu/>)<sup>35</sup>. The topography is based on the ETOPO1 1 Arc-Minute Global Relief Model, <http://www.ngdc.noaa.gov/mgg/global/global.html><sup>36</sup>.

The adopted GMPE is obtained from the analysis of the Italian earthquakes and is valid for magnitude ranging between 4.0 and 6.9 and distances up to 200 km (ref. 7).

From the analysis of the cumulative stress transfer ( $\Delta\text{CFS}$ ) we argue that its effect at the locations and on the focal mechanisms of the largest subsequent earthquakes does not explain their occurrence. Indeed, for the first five main events, the corresponding  $\Delta\text{CFS}$  values are one order of magnitude smaller than the minimum  $\Delta\text{CFS}$  commonly required to significantly contribute to the triggering process alone (i.e., 0.01 MPa)<sup>8,9</sup> (supplementary Figure S1 and also Figure 3a). This statement holds regardless of whether we consider the preferential nodal plane (inferred from geological information, i.e. E-W striking, S-dipping<sup>1,10</sup>) or the auxiliary one. Additionally, since static stress redistribution is commonly characterized by symmetrical lobes of positive and negative values around the seismic source, it makes difficult to identify any preferred direction for subsequent event locations. Moreover, the symmetry of

the static stress fields also differs from the asymmetries in the after-shock patterns.

Summarizing, although static stress changes may affect the evolution of this sequence, they not appear to be significant contributors to the triggering process. In the following of our study, we try to overcome the aforementioned limitation of the static Coulomb model by combining the source rupture directivity and the dynamic strain field.

Previous studies<sup>11–19</sup> also have noted the influence of the rupture direction in the dynamic stress field for large and small-to-moderate earthquakes.

We analysed the major events that occurred during the sequence (Table 1 and Figure 1) by considering only those earthquakes for which focal mechanisms and/or aftershock distributions are available. We identified the horizontal rupture directions  $\phi$  and estimated the Mach numbers  $\alpha$  (i.e., the ratio between rupture and shear-wave velocities) through the inversion of PGVs<sup>20,21</sup>. We show in Figure 2

**Table 1 | Source parameters of the main earthquakes of the Emilia seismic sequence**

Event	Hypocentral location					Mw	$\phi$	$\delta$	$\lambda$	$\phi_D$	$\phi_S$
	Date	Time	Lat(N)	Long(E)	Depth(km)						
1	05/20/2012	02:03:52	44.889	11.228	6.0	5.6	105/285	45/45	90/90	$102 \pm 12$	$286 \pm 12$
2*	05/20/2012	02:07:31	44.863	11.370	5.0	5.1	77/252	37/53	94/87	$298 \pm 35$	$98 \pm 49$
3	05/20/2012	03:02:50	44.860	11.095	13.0	4.7	132/245	50/65	147/45	$80 \pm 24$	-
4	05/20/2012	13:18:02	44.831	11.490	7.0	4.8	120/275	38/55	110/75	$292 \pm 26$	$110 \pm 21$
5	05/29/2012	07:00:03	44.851	11.086	5.0	5.4	97/270	45/45	95/85	$304 \pm 22$	$116 \pm 20$
6	05/29/2012	10:55:57	44.888	11.008	6.0	5.1	96/282	40/50	85/94	$278 \pm 73$	-
7*	05/29/2012	11:00:25	44.8790	10.9470	5.4	5.2	77/252	37/53	94/87	$106 \pm 41$	-
8	06/03/2012	19:20:43	44.899	10.943	10.0	4.6	117/265	29/65	119/75	$76 \pm 24$	$208 \pm 38$

Hypocentral location, moment magnitude, and fault plane solution (strike,  $\phi$ , dip,  $\delta$ , and rake,  $\lambda$ , for the principal and auxiliary planes) of the main earthquakes of the Emilia seismic sequence<sup>3</sup>. For the events marked by an asterisk, locations are taken from the INGV catalog (<http://iside.rm.ingv.it>) and focal mechanisms are an average of the all 22 known focal mechanisms<sup>3</sup>. The last two columns list the dominant ( $\phi_D$ ) and secondary ( $\phi_S$ ) rupture directions, respectively, estimated from the PGVs inversion. The uncertainties on  $\phi_D$  and  $\phi_S$  have been evaluated measuring the Half Width at Half Maximum of the best-model Pdfs shown in Figure S2.

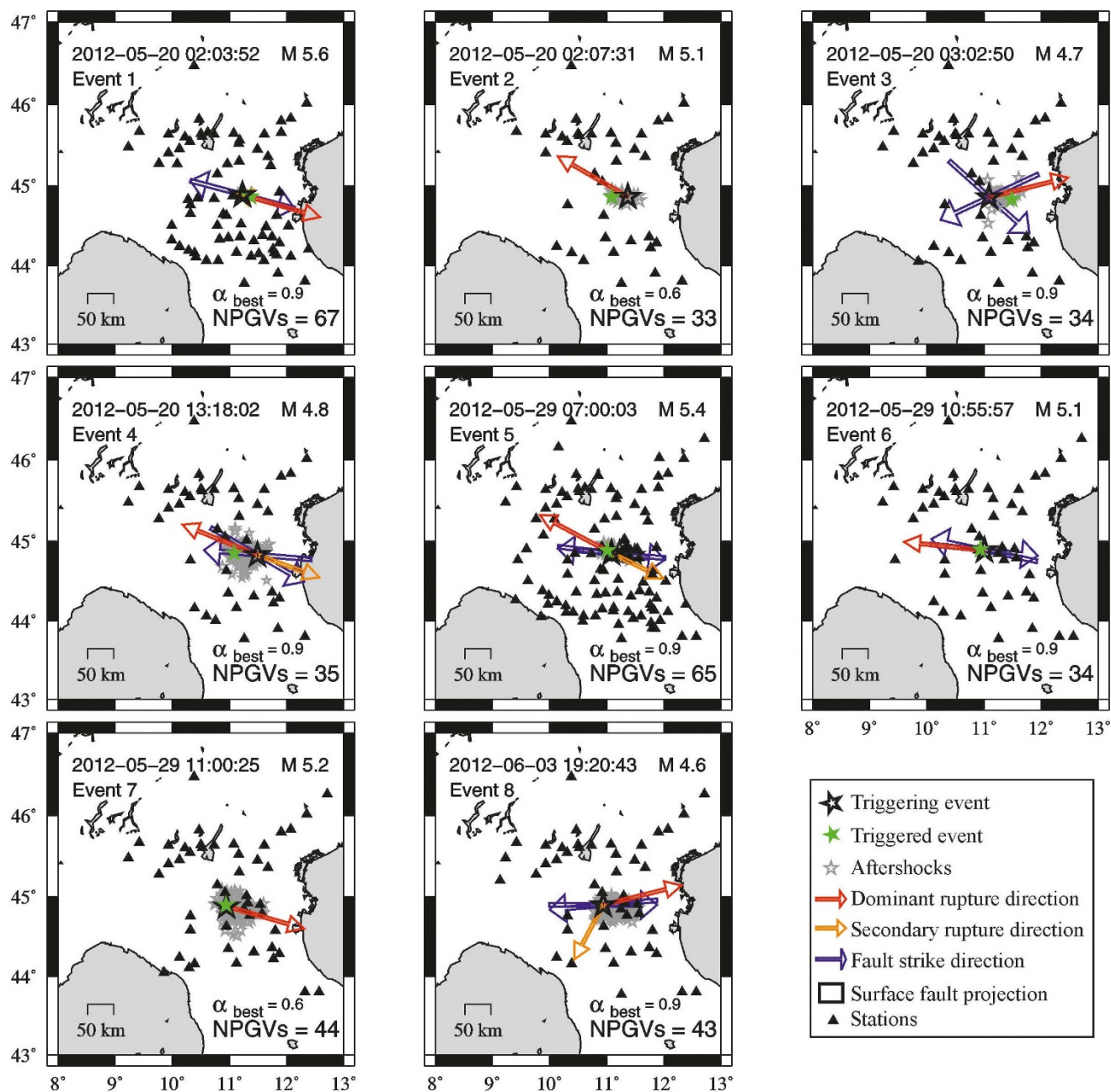


**Figure 2 | Maps of dominant rupture direction.** Overview of inferences obtained from the inversion of the peak-ground velocities for the main triggering events (black stars) considered in this study. In each panel, the dominant rupture directions (red arrows) and aftershock distributions (gray stars) up-to the next main event in the sequence (green stars), are shown. The orange arrow indicates the secondary rupture direction and its length depends on the ratio between the Pdf at the secondary maximum and the value at the absolute maximum (supplementary Figure S2). The uncertainties of the rupture directions are given in Table 1. The blue arrows indicate strike directions of the principal and auxiliary fault planes deduced from the corresponding focal mechanism<sup>3</sup>. The black triangles identify the stations at which PGVs data were available. In each panel the origin time and magnitude of the triggering event are specified, as well as the best value of the Mach number  $\alpha$  and the available number of PGV data used. The figure was generated by using the Generic Mapping Tools (<http://gmt.soest.hawaii.edu/>)<sup>35</sup>.

locations of triggering events, their dominant rupture directions and aftershocks distribution occurred up-to the next event in the sequence. From a visual inspection, a correlation is evident: we observe that for each main earthquake its aftershocks and the subsequent main event occur in the areas oriented as the source dominant rupture direction.

The probability density functions (Pdfs) of  $\phi$  (supplementary Figure S2) are analysed to assess the reliability of the retrieved rupture direction. The uncertainties, evaluated as the Half Width at Half Maximum of the Pdfs corresponding to the best model, are of the

order of 10–40 degrees (Table 1). In some cases (e.g., events 4, 5 and 8) the  $\phi$ -Pdfs present a secondary mode that indicates a deviation from a purely unilateral rupture. Note that we consider the secondary maximum only if it differs more than 90 degrees from the principal one. For the aforementioned events the Pdfs on the percent unilateral rupture parameter  $e$  (see Method section for its formal definition) also suggest a quasi-bilateral rupture propagation on the fault plane. It is worth noting that we find different best-fit Mach number  $\alpha$  that either 0.6 or 0.9. This result may be attributed to a variation in the rupture velocity rather than a variation in the shear-wave velocity. Indeed,

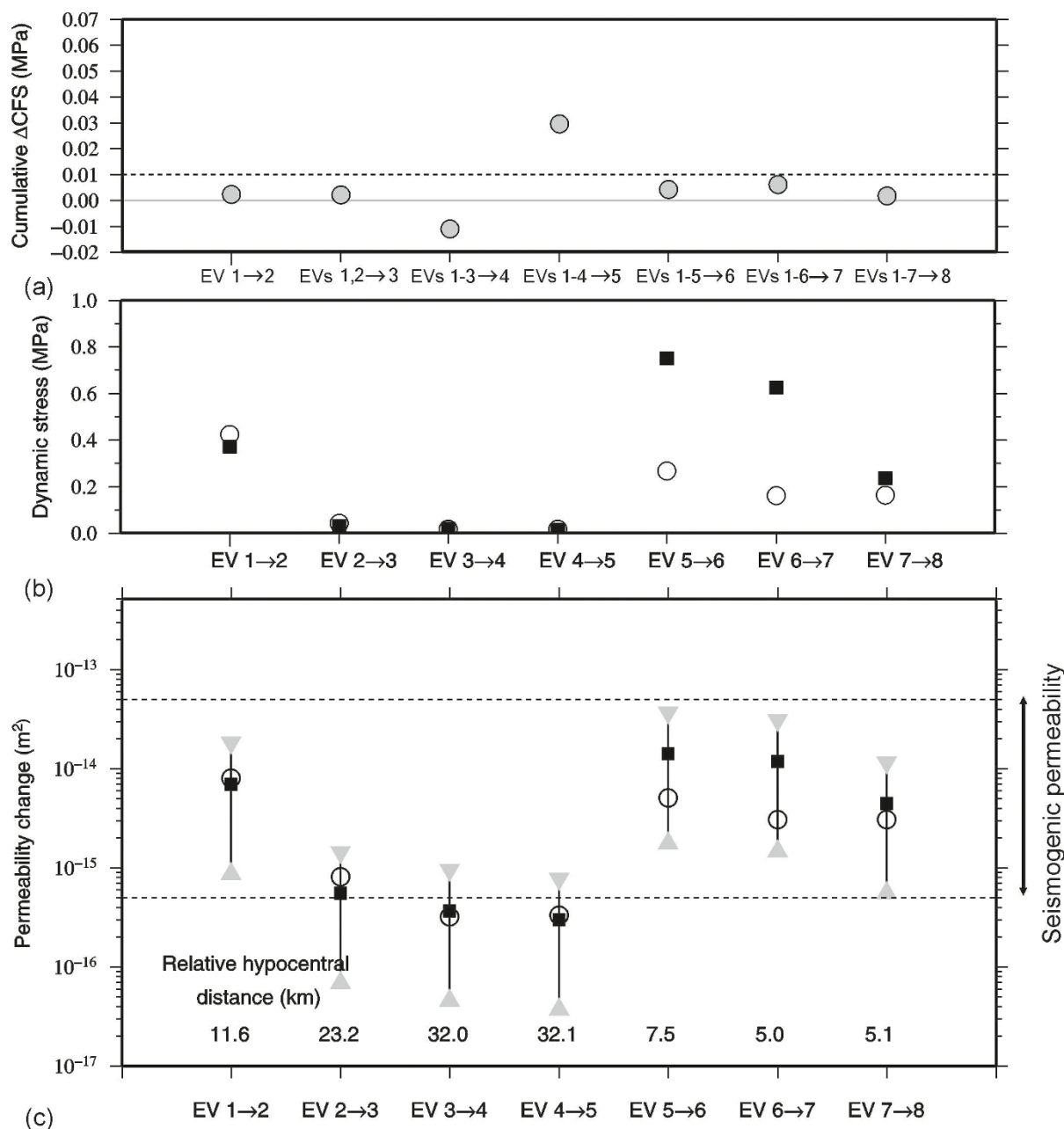


**Figure 3 | Static and dynamic stress transfer and permeability change.** Panel (a): local cumulative  $\Delta CFS$  at hypocentral locations and on preferential focal mechanisms of target main events. Cumulative  $\Delta CFS$  is estimated considering the contribution of all the earthquakes occurred before the target event. The dataset used for Coulomb stress estimation contains 22 events for which locations and focal mechanisms are available<sup>3</sup>. For the events 2 and 7 in Table 1 the fault plane solutions are not available and a mean focal mechanism is then assumed. The dashed line represents the commonly accepted triggering threshold for static  $\Delta CFS$ <sup>8,9</sup>. Below this threshold, stress changes are considered too small to significantly contribute to the triggering process. Panel (b): local dynamic stress change obtained from the peak dynamic strain (assuming a rigidity value of 30 GPa) induced by each considered event at the hypocenter of the next main earthquake in the sequence. The local dynamic stress is estimated both considering the directivity function  $C_d$  (squares) and ignoring it (open circles). Panel (c): permeability change  $\Delta K$  induced by each considered event at the hypocenter of the next main earthquake in the sequence. The two horizontal dashed lines define the seismogenic permeability range ( $5 \times 10^{-16} - 5 \times 10^{-14} m^2$ )<sup>27,28</sup>.  $\Delta K$  changes are estimated through PGV values: i) modified by the source directivity function  $C_d$  (squares); and ii) not modified by  $C_d$  (open circles). The gray triangles represent  $\Delta K$  obtained by using the upper and lower  $R$  bounds (see equation 2). The relative hypocentral distance (in km) between each triggering and target events, is provided in the bottom of the panel. In the three panels, the numbering on x-axis refers to the seismic events as listed in Table 1.

rupture velocity variations produce a different ground-motion field: the faster the rupture, the larger the ground-motion amplitudes<sup>22–24</sup>.

PGVs can be also used to estimate the peak-dynamic strain field<sup>18</sup>. We use the directivity function  $C_d$  (see Method section) to account for modifications of PGVs due to source directivity while computing the dynamic strain field.

Figure 4 shows that the major events of the Emilia seismic sequence occurred in areas where the peak-dynamic strain values are in the range of the dynamic triggering<sup>12</sup> (from a few microstrain up to tens of microstrain). Moreover, the corresponding local dynamic stress changes ( $\sim 0.1$ – $1$  MPa, assuming a rigidity of 30 GPa) are about one order of magnitude higher than the cumulative static



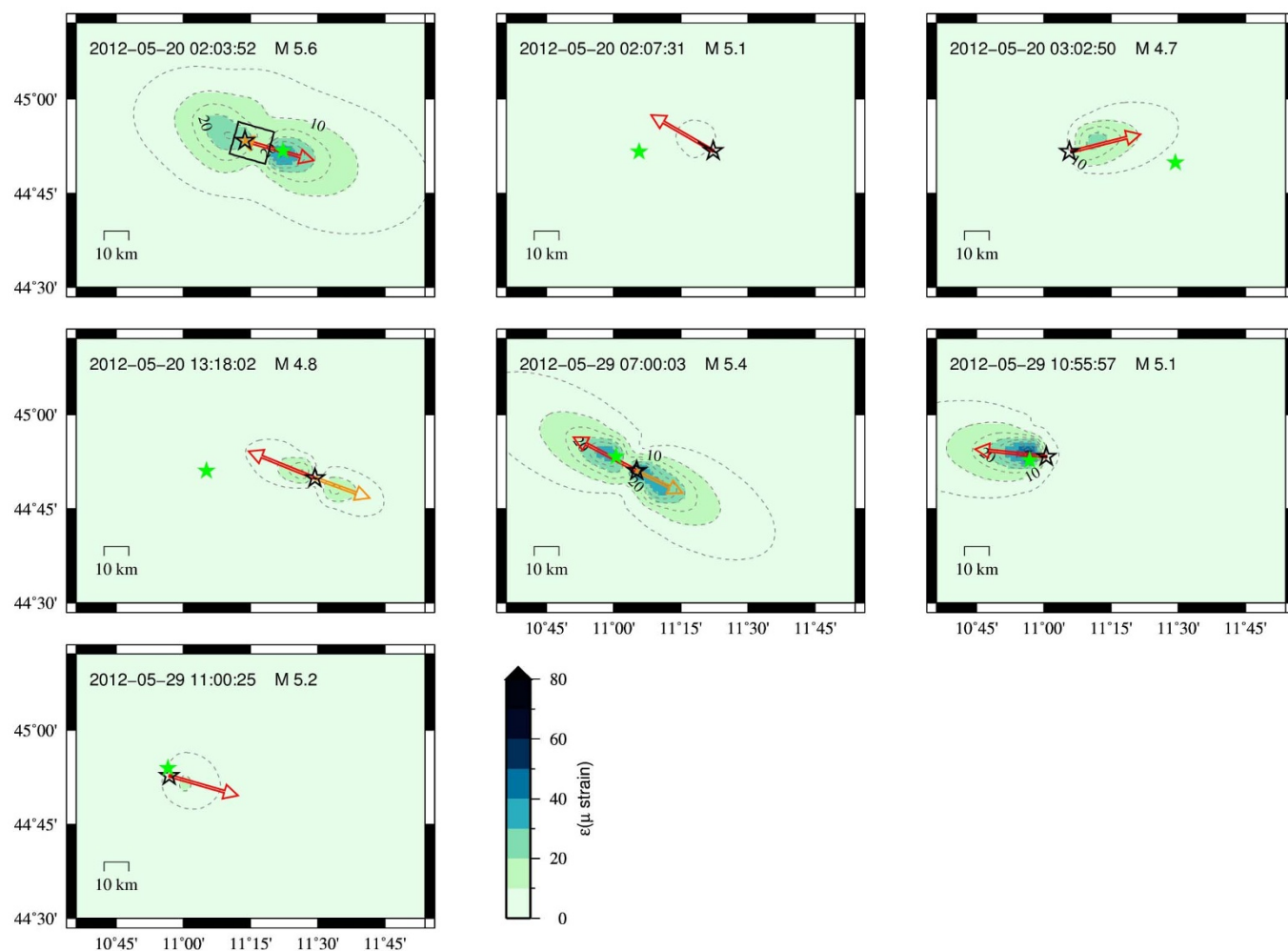


**Figure 4 | Geographical distribution of peak-dynamic strain.** Peak-dynamic strain field (microstrain) obtained by using the peak-ground velocity as a proxy ( $\epsilon \approx PGV/V_s$ ). In each panel, the black and green stars indicate the triggering and target event, respectively. The red and orange arrows represent the dominant and the secondary rupture directions, respectively. Black rectangles represent the surface fault projections estimated through PGVs inversion (in some cases dimensions are very small and then dimly visible).

stress changes (Figure 3b and 3a). This might suggest that the dynamic effect played a significant role in the evolution of this seismic sequence.

Furthermore, we analyse the variation of the permeability,  $\Delta k$ , in the fractured area. Permeability variations are also associated with the passage of seismic waves, which indeed increase pore pressure and fluid-flow rates in a fluid-saturated medium<sup>25</sup>. The presence of fluids in the Emilia region has been suggested in a tomographic study that found a high  $V_p$  and high  $V_p/V_s$  ratio (about 1.814) for the area, which indicates a fluid-saturated and partially-fractured medium<sup>26</sup>. Our idea is that source directivity can also enhance changes in permeability. Such variations of permeability might encourage the fracture in a preferred direction as a consequence of a local increase of the pore pressure and fluid flow rates, resulting in a reduction of the effective normal stress. For each main event we evaluate the change in permeability at the location of the next earthquake in the sequence. For all the considered events, the induced  $\Delta k$  values are in the range of the seismogenic permeability<sup>27,28</sup> (from  $5 \times 10^{-16} \text{ m}^2$  to  $5 \times 10^{-14} \text{ m}^2$ ) (Figure 3c) and can then be associated with the evolution of the seismic sequence.

## Discussion

This study indicates that the dynamic triggering caused by passing seismic waves and enhanced by source directivity might be the

primary factor to explain the evolution of the 2012 Emilia seismic sequence. In fact, we observed a correlation between the locations of aftershocks and subsequent main events with: i) the peak dynamic strain fields; ii) the local change of the permeability.

We also observe that static Coulomb stress changes did not play a significant role, remaining under the threshold value for static triggering.

The correlation between variations of permeability and location of events suggests that the presence of fluids might contribute to the evolution of the sequence by altering the effective normal stress in specific areas.

We think that this issue deserves future research to be used to improve the forecasting ability of models based on stress change.

## Methods

We estimate the surface fault projection and the dominant horizontal rupture direction of the analysed earthquakes through an inversion technique of PGVs. This technique minimizes the difference between observed and predicted PGV values using a grid-searching scheme in a Bayesian framework<sup>20</sup>. Peak predictions are obtained from a GMPE by using the  $R_{JB}$  distance (i.e., the minimum distance of a site from the surface fault projection) metric<sup>29</sup>. A first order correction for site effects is obtained through a method<sup>30</sup> that uses the value of the average shear-wave velocity over the uppermost 30 m (VS30) and provides with multiplicative coefficients. The VS30 values have been extracted from the database compiled for implementing ShakeMap in Italy<sup>6</sup>. Predictions including site effect are then modified to account for the source directivity through the directivity function  $C_d$  given by



$$C_d = \frac{1}{2} \sqrt{\frac{(1+e)^2}{(1-\alpha \cos \vartheta)^2} + \frac{(1-e)^2}{(1+\alpha \cos \vartheta)^2}}, \quad (1)$$

where  $\vartheta$  is the angle between the ray leaving the source and the direction of rupture propagation  $\phi^{31}$ , and  $\alpha$  is the Mach number. The percent unilateral rupture  $e$ , is defined as  $(2L' - L)/L$ , where  $L$  is the fault length and  $L'$  the prevalent rupture direction<sup>17</sup>. It allows for the discrimination between unilateral ( $e = 1$ ) and bilateral ( $e = 0$ ) ruptures.

Details on the inversion technique are provided in the paper in which the method has been originally presented<sup>20</sup>. Here, we just note that the best solution for surface fault projection, and for  $\phi$  and  $e$ , corresponds to the largest value of the a-posteriori Pdfs resulting from the adopted Bayesian approach. The associated standard error are obtained by analysing the marginal Pdfs.

As we have analysed a sequence of earthquakes characterized by different (moderate) magnitude, we expect that  $\alpha$  might not be the same for all the events. Thus, for each earthquake we inverted PGV values by exploring  $\alpha$  in the range 0.2–0.9 with a 0.1 increment. The smallest residual value allows us to select the best model.

The estimation of the peak dynamic strain ( $\varepsilon$ ) field is based on an empirical approach that uses PGVs as a proxy:  $\varepsilon \approx PGV/V_s$ , where  $V_s$  is the shear-wave velocity<sup>18</sup>. PGVs predicted by using the GMPE are here modified by the  $C_d$  coefficient and divided by a factor of 2 in order to correct for the free-surface amplification<sup>32</sup>.

We estimate variations in the permeability factor through the relationship<sup>25</sup>:

$$\Delta k = R \frac{PGV \cdot C_d}{V_s}, \quad (2)$$

The coefficient  $R$  accounts for the strain effect on the permeability response and ranges between  $3.0 \times 10^{-10} \text{ m}^2$  and  $8.4 \times 10^{-10} \text{ m}^2$  (ref. 25) with a central value of  $5.7 \times 10^{-10} \text{ m}^2$ , which has been used in our study. As for the strain field computation, the PGVs account for the directivity function  $C_d$  and free-surface amplification. Both for peak dynamic strain field and for permeability factor computation, the  $V_s$  values at each earthquake hypocenter have been estimated from a tomographic velocity model valid for the Emilia region<sup>26</sup>.

Coulomb static stress variations,  $\Delta CFS$ , are computed by using the solutions for a homogeneous elastic half-space<sup>33</sup>. The Coulomb model is commonly defined as  $\Delta CFS = \Delta \tau + \mu' \Delta \sigma$ , where  $\Delta \tau$  is the shear stress change on the failure plane (positive in the slip direction),  $\Delta \sigma$  is the effective normal stress change (positive for extension) and  $\mu'$  is the apparent friction coefficient<sup>34</sup>. We estimated dimensions and mean slip of extended square fault patches by using scaling relationships<sup>4,5</sup> and assuming a constant stress drop of 2.4 MPa on the faults, which is approximately the average value retrieved for the study area from the analysis of strong-motion records<sup>35</sup>.

In the present study we used a friction coefficient  $\mu = 0.8$  (common to almost all the type of rocks), a Skempton ratio  $B = 0.5$ , and a rigidity value of 30 GPa.

- Ventura, G. & Di Giovambattista, R. Fluid pressure, stress field and propagation style of coalescing thrusts from the analysis of the 20 May 2012 ML 5.9 Emilia earthquake (Northern Apennines, Italy). *Terra Nova* **25**, 72–78, doi:10.1111/ter.12007 (2013).
- Lindquist, S. J. Petroleum Systems of the Po Basin Province of Northern Italy and the Northern Adriatic Sea: Porto Garibaldi (Biogenic), Meride/Riva di Solto (Thermal), and Marnoso Arenacea (Thermal). USGS Open-File Report 99-50-M (1999).
- Malagnini, L. *et al.* The 2012 Ferrara seismic sequence: Regional crustal structure, earthquake sources, and seismic hazard. *Geophys. Res. Lett.* **39**, L19302, doi:10.1029/2012GL053214 (2012).
- Hanks, T. C. & Kanamori, H. A moment-magnitude scale. *J. Geophys. Res.* **84**, 2348–2350 (1979).
- Keilis-Borok, V. On estimation of the displacement in an earthquake source and of source dimensions. *Ann. Geophys.* **12**, 205–214 (1959).
- Michellini, A., Faenza, L., Lauciani, V. & Malagnini, L. ShakeMap implementation in Italy. *Seismol. Res. Lett.* **79**, 688–697, doi:10.1785/gssrl.79.5.688 (2008).
- Bindi, D. *et al.* Ground Motion Prediction Equations derived from the Italian strong motion data base. *Bull. Earth. Eng.* **9**, 1899–1920, doi:10.1007/s10518-011-9313-z (2011).
- Reasenber, P. A. & Simpson, R. W. Response of regional seismicity to the static stress change produced by the Loma Prieta earthquake. *Science* **255**, 5052, 1687–1690, DOI:10.1126/science.255.5052.1687 (1992).
- Hardebeck, J., Nazareth, J. & Hauksson, E. The static stress change triggering model: Constraints from two southern California aftershock sequences. *J. Geophys. Res.* **103**(B10), 24,427 (1998).
- Basili, R. *et al.* The Database of Individual Seismogenic Sources (DISS), version 3: summarizing 20 years of research on Italy's earthquake geology. *Tectonophysics* **453**, 20–43, doi:10.1016/j.tecto.2007.04.014 (2008).
- Mohamad, R. *et al.* Remote earthquake triggering along the Dead Sea Fault in Syria following the 1995 Gulf of Aqaba earthquake ( $M_s = 7.3$ ). *Seismol. Res. Lett.* **71**, 47–52 (2000).
- Gomberg, J., Reasenber, P. A., Bodin, P. & Harris, R. A. Earthquake triggering by seismic waves following the Landers and Hector Mine earthquakes. *Nature* **411**, 462–466 (2001).

- Kilb, D., Gomberg, J. & Bodin, P. Triggering of Earthquake Aftershocks by Dynamic Stresses. *Nature* **408**, 570–574 (2000).
- Kilb, D. A strong correlation between induced peak dynamic Coulomb stress change from the 1992 M7.3 Landers, California, earthquake and the hypocenter of the 1999 M7.1 Hector Mine, California, earthquake. *J. Geophys. Res.* **108**(B1), 2012, doi:10.1029/2001JB000678 (2003).
- Gomberg, J., Bodin, P. & Reasenber, P. A. Observing Earthquakes Triggered in the Near Field by Dynamic Deformations. *Bull. Seismol. Soc. Am.* **93**, No. 1, 118–138 (2003).
- Gomberg, J. & Bodin, P. Triggering of the Little Skull Mountain, Nevada earthquake with dynamic strains. *Bull. Seismol. Soc. Am.* **84**, 844–853 (1994).
- Boatwright, J. The persistence of directivity in small earthquakes. *Bull. Seismol. Soc. Am.* **97**, 1850–1861 (2007).
- van der Elst, N. J. & Brodsky, E. E. Connecting near-field and far-field earthquake triggering to dynamic strain. *J. Geophys. Res.* **115**, B07311, doi:10.1029/2009JB006681 (2010).
- Cotton, F. & Coutant, O. Dynamic stress variations due to shear faults in a plane-layered medium. *Geophysical Journal International* **128**, 676–688, doi:10.1111/j.1365-246X.1997.tb05328.x (2012).
- Convertito, V. *et al.* Fault Extent Estimation for Near-Real-Time Ground-Shaking Map Computation Purposes. *Bull. Seismol. Soc. Am.* **102**, 2, 661–679; doi:10.1785/0120100306 (2012).
- Convertito, V. & Emolo, A. Investigating Rupture Direction for Three 2012 Moderate Earthquakes in Northern Italy from Inversion of Peak-Ground Motion Parameters. *Bull. Seismol. Soc. Am.* **102**, 6, 2764–2770, doi:10.1785/0120120067 (2012).
- Emolo, E. *et al.* Ground motion scenarios for the 1997 Colfiorito, central Italy, earthquake. *Ann. Geophys.* **51**, N 2/3, 509–525 (2008).
- Cultrera, G., Pacor, F., Franceschina, G., Emolo, A. & Cocco, M. Directivity effects for moderate-magnitude earthquakes ( $M_w$  5.6–6.0) during the 1997 Umbria-Marche sequence, central Italy. *Tectonophysics* **476**, 110–120, doi:10.1016/j.tecto.2008.09.022 (2009).
- Mai, P. M. Ground Motion: Complexity and Scaling in the Near Field of Earthquake Ruptures. In Lee, W. H. K. & Meyers, R. editors, *Encyclopedia of Complexity and Systems Science*, pages 4435–4474. Springer (2009).
- Elkhoury, J. E., Brodsky, E. E. & Agnew, D. C. Seismic waves increase permeability. *Nature* **441**, 1135–1138, doi:10.1038/nature04798 (2006).
- Ciaccio, M. G. & Chiarabba, C. Tomographic models and seismotectonics of the Reggio Emilia region, Italy. *Tectonophysics* **344/3–4**, 261–276 (2002).
- Talwani, P., Chen, L. & Gahalaut, K. Seismogenic permeability, ks. *J. Geophys. Res.* **112**, B07309, doi:10.1029/2006JB004665 (2007).
- El Hariri, M., Abercrombie, R. E., Rowe, C. A. & Do Nascimento, A. F. The role of fluids in triggering earthquakes: observations from reservoir induced seismicity in Brazil. *Geophysical Journal International* **181**, 1566–1574. doi:10.1111/j.1365-246X.2010.04554.x (2010).
- Joyner, W. B. & Boore, D. M. Peak horizontal acceleration and velocity from strong-motion records including records from the 1979 Imperial Valley, California, earthquake. *Bull. Seismol. Soc. Am.* **71**, 2011–2038 (1981).
- Wald, D. J. & Allen, T. I. Topographic slope as a proxy for seismic site conditions and amplification. *Bull. Seismol. Soc. Am.* **97**, 1379–1395 (2007).
- Joyner, W. B. Directivity for non-uniform ruptures. *Bull. Seismol. Soc. Am.* **81**, 1391–1395 (1991).
- Douglas, J. Estimating strong ground motion at great depths. Third International Symposium on the Effects of Surface Geology on Seismic Motion Grenoble, France, 30 August–1 September 2006 Paper Number: 30 (2006).
- Okada, Y. Internal deformation due to shear and tensile faults in a half-space. *Bull. Seismol. Soc. Am.* **82**(2), 1018–1040 (1992).
- Harris, R. A. Introduction to Special Section: Stress Triggers, Stress Shadows, and Implications for Seismic Hazard. *J. Geophys. Res.* **103**(B10), 24347–24358, doi:10.1029/98JB01576 (1998).
- Wessel, P. & Smith, W. H. F. Free software helps map and display data, EOS Trans. AGU **72**, 441, 445–446 (1991).
- Amante, C. & Eakins, B. W. ETOPO1 1 Arc-Minute Global Relief Model: Procedures, Data Sources and Analysis. NOAA Technical Memorandum NESDIS NGDC-24, 19 pp, March (2009).

## Acknowledgements

We wish to thank Simona Pierdominici for useful discussions on the main geological characteristics of the study area, her positive criticism and review of Figures. We thank Luca D'Auria for valuable discussions on the dynamic strain and Laura Scognamiglio for the recognition of the best current dataset to use for calculations. We are grateful to Jeremy Douglas Zechar for editing the first version of the manuscript. We are also grateful to the Editor Tim Wright and to anonymous reviewers for their valuable comments and careful review. All the Figures are generated by using the Generic Mapping Tools (<http://gmt.soest.hawaii.edu/>)<sup>35</sup>. The topography in Figure 1 is based on the ETOPO1 1 Arc-Minute Global Relief Model, <http://www.ngdc.noaa.gov/mgg/global/global.html><sup>36</sup>. This research was partially supported by the EU-FP7 project REAKT (Strategies and tools for real time earthquake risk reduction).



### Author contributions

V.C., F.C. and A.E. all promoted the study, and contributed to result interpretation and paper writing. V.C. produced the results for the directivity effect. F.C. produced the Coulomb static stress transfer results.

### Additional information

Supplementary information accompanies this paper at <http://www.nature.com/scientificreports>

**Competing financial interests:** The authors declare no competing financial interests.

**How to cite this article:** Convertito, V., Catalli, F. & Emolo, A. Combining stress transfer and source directivity: the case of the 2012 Emilia seismic sequence. *Sci. Rep.* 3, 3114; DOI:10.1038/srep03114 (2013).



This work is licensed under a Creative Commons Attribution-NonCommercial-NoDerivs 3.0 Unported license. To view a copy of this license, visit <http://creativecommons.org/licenses/by-nc-nd/3.0>